NJC

Cite this: *New J. Chem.*, 2012, **36**, 161–167

www.rsc.org/njc

PAPER

Catalytic performance of lanthanide molecular solids containing well-modified metal–organic octahedra†

Xiao Wu, Zhihua Lin, Cheng He* and Chunying Duan

Received (in Montpellier, France) 24th August 2011, Accepted 28th October 2011
DOI: 10.1039/c1nj20736a

Channel-like and cage-like porous molecular materials Tb–**PT1** and Sm–**PT1** were constructed through packing and stacking of the amide-containing lanthanide-based octahedra $[Tb_6(H_3L)_4(NO_3)_9\text{-}3H^+]^{6+}$ and $[Sm_6(H_3L)_4(NO_3)_{12}]^{6+}$, respectively, where H_3L is *N*′,*N*′,*N*′′-tris(pyridin-2-ylmethylene)benzene-1,3,5-tricarbohydrazide. Catalytic experiments on cyanosilylation reactions exhibited that the loading of only 1 mol% of Tb–**PT1** leads to >90% conversion of the products with all the three nitrobenzaldehydes (**NBA**), but less than 10% conversion in the case of large size 3-formyl-1-phenylene-3 and 5-di-*tert*-butylbenzoate (**BA**) substrates. Adsorption of the substrates in the catalyst demonstrated a 3 : 1 mole ratio (per octahedron) of these nitrobenzaldehydes, but no adsorption of **BA** could be observed. Luminescent detection of the suspension of Tb–**PT1** in CH_2Cl_2 solution exhibited that the presence of nitrobenzaldehydes quenched the emissions efficiently, whereas the addition of **BA** did not cause any significant spectra variations. All these results revealed that the catalytic performance of Tb–**PT1** was size-selective and the interactions corresponding to the Tb^{3+} sites were dominant in activating the aldehydes. The catalytic experiments on aldol reactions between cyclohexanone and these aldehydes exhibited that the smallest 4-**NBA** substrate has the largest conversion (80%) over the others. The presence of cyclohexanone led to absorption spectral changes and luminescence enhancements of the catalyst. These results suggested that interactions between cyclohexanone and the amide groups were dominant in activating the cyclohexanone and the aldol reactions possibly occurred within the cavities of the octahedron. Evaluation of catalytic performance of Sm–**PT1** in which those channels in Tb–**PT1** were blocked upon cyanosilylation and aldol reactions as well as the adsorption experiments were also carried out for a comparison.

Introduction

Metal–organic polyhedra (MOPs), discrete molecular architectures constructed through the coordination of metal ions and organic linkers, have attracted considerable attention due to their high symmetry, stability and rich chemical/physical properties potential for a variety of applications.[1,2] These molecules are synthesized by using modular and high yield metal directed self-assembly methods, so that the geometric and electronic characteristics embedded within the individual components have collectively allowed the construction of the supramolecular entities in a controllable way.[3,4] These structures discussed exhibit well-defined cavities with gated pores providing specific inner environments for selective uptaking and binding of guest molecules. Many of them exhibit reactivity and specificity reminiscent of natural systems, and some of them have functions that exceed the natural systems which provided the inspiration for initially making them.[5,6] For example, the special micro-environment in the cage-compounds of Raymond *et al.*[7] increases dramatically the acid-catalyzed hydrolysis reaction of orthoesters even in a basic reaction medium. Fujita applied the typical M_6L_4 cage-compounds in Diels–Alder reactions to obtain unique products through the cage-directed selectivity effect.[8] These recent breakthroughs also demonstrate that the implementation of supramolecular strategies in traditional homogeneous catalysis approaches serves as a powerful tool to solve problems in the field of homogeneous catalysis.[9]

The immobilization of homogeneous catalysts on solid supports represents an established field that is on the verge of being applied in industry,[10] and the emerging young field of microporous metal–organic frameworks (MOFs) has attracted wide attention for their superior functional properties and applications in heterogeneous catalysis.[11] The use of metal–organic macrocycles as molecular building blocks for the creation of extesively porous materials has implications for a whole generation of heterogeneous catalysts. Since the molecules defining the cavities conceivably align and stack in the solid state to create semi-infinite

State Key Laboratory of Fine Chemicals, Dalian University of Technology, Dalian 116024, China. E-mail: hecheng@dlut.edu.cn
† Electronic supplementary information (ESI) available. CCDC 675067. For ESI and crystallographic data in CIF or other electronic format see DOI: 10.1039/c1nj20736a

channel structures, these materials would be expected to typically display the combined advantages of homogeneous and heterogeneous catalyses,[12] such as high activity and selectivity on the one hand, and easy separation and efficient recycling, on the other, that result in an overall lower cost compared to others.[13] The ready tenability of such an approach is also expected leading to unique and useful heterogeneous catalysis, since the rigid and shape-persistent metal–organic macrocycles are versatile building blocks for supramolecular design and are possibly suited for the hierarchical assembly of porous materials with utilizable functional groups.

Through carefully incorporating amide groups as guest-accessible functional organic sites within the well-defined metal–organic architectures, researchers, including us, have reported a powerful approach to assemble metal-tunable Werner-type cages composed of transition metal and lanthanide ions for size- or shape-selective dynamic molecular sensing.[14] In several recent discoveries, amide-containing metal–organic polyhedra (MOPs)[13c,15] and MOFs[16] were found to be capable of prompting chemical reactions efficiently. Since the coordinated unsaturated lanthanide ions are also able to function as active catalysis sites for acid promoting reactions,[17] we envisioned that the assembled metal–organic polyhedra containing both potential unsaturated lanthanide ions and amide groups should exhibit efficient base-type and acid-type catalytic performances at the same time. To realize the above-mentioned postulation, herein we investigate the preparation of porous materials through the packing and stacking of the amide-containing lanthanide-based octahedra Tb–**PT1** and Sm–**PT1** in the crystalline solid[14] and validate the catalytic properties in cyanosilylation reactions and aldol reactions, respectively.

Experimental

Instruments and reagents

All chemicals were of reagent grade quality, obtained from commercial sources and used without further purification. The elemental analyses of C, H and N were performed on a Vario EL III elemental analyzer. ^{1}H NMR spectra were measured on a Varian INOVA 400 M spectrometer. The powder XRD diffractograms were obtained on a RigukuD/Max-2400 X-ray Diffractometer with a Cu sealed tube (λ = 1.54178 Å).

Preparation of Tb–PT1

The synthetic procedure of complex Tb–**PT1** has been reported in our previous work.[14] Anal. calc. for $Tb_6(C_{108}H_{81}N_{36}O_{12})(NO_3)_{15}(H_2O)$, H 2.10, C 32.62, N 17.96%; found: H 2.70, C 32.12, N 17.43%. ^{1}H NMR (DMSO-d_6, ppm): 12.48 (s, 9H, H_2), 8.63 (br, 36H, H_3, H_7, H_1), 8.04 (br, 24H, H_4, H_5), 7.45 (br, 12H, H_6). IR (KBr plate): 3421 (br, υ_{N-H} and υ_{O-H}), 1636 (m, $\upsilon_{C=O}$ and $\upsilon_{C=N}$), 1560, 1517, 1476 (w, $\upsilon_{Ar-C=C-}$ and $\upsilon_{Ar-C=N-}$), 1384 (s, υ_{NO3}), 1300 (m, υ_{C-N}).

Preparation of Sm–PT1

A solution of $Sm(NO_3)_3{\cdot}6H_2O$ (0.033 g, 0.075 mmol) in methanol (6 mL) was layered onto a solution of **PT1** ligand (0.026 g, 0.05 mmol) in $CH_3OH/CHCl_3$ (v : v = 1 : 4, 6 mL). The solution was left for one week at room temperature to give X-ray quality yellow block crystals. Yield: about 62% based on the crystals that have been collected and then dried in vacuum. Anal. calc. for $Sm_6(C_{27}H_{21}N_9O_3)_4(NO_3)_{18}$, H 2.07, C 31.67, N 18.46%; found: H 2.55, C 30.94, N 17.80%. ^{1}H NMR (DMSO-d_6, ppm): 12.49 (s, 12H, H_2), 8.65 (m, 36H, H_3, H_7, H_1), 8.05 (d, 12H, H_4, J = 7.2 Hz), 7.93 (t, 12H, H_5, J = 15.3 Hz), 7.47 (t, 12H, H_6, J = 11.7 Hz). IR (KBr plate): 3398 (br, υ_{N-H} and υ_{O-H}), 1636 (m, $\upsilon_{C=O}$ and $\upsilon_{C=N}$), 1560, 1516, 1474, 1439 (w, $\upsilon_{Ar-C=C-}$ and $\upsilon_{Ar-C=N-}$), 1384 (s, υ_{NO3}), 1297 (*m*, υ_{C-N}).

General procedure for the aldol reaction

Compound Tb–**PT1** or Sm–**PT1** (10 μmol) was added to a suspension of aldehyde (0.5 mmol), cyclohexanone (0.52 mL, 5 mmol), water (0.5 mL) and CH_3OH (0.5 mL) at 37 °C. The reaction mixture was stirred for 5 d and EtOAc (5 mL) was added. The filtrate was dried (Na_2SO_4) and concentrated in a vacuum. The conversion and diastereomer were determined by ^{1}H NMR analysis of the crude aldol products.

General procedure for the cyanosilylation of aldehyde substrates

Compound Tb–**PT1** or Sm–**PT1** (5 μmol) was added to a suspension of aldehyde (0.5 mmol), Me_3SiCN (0.594 g, 0.6 mmol) and dry dichloromethane (0.5 mL) at 20 °C. The reaction mixture was stirred for 1.5 h and dry dichloromethane (5 mL) was added. The filtrate was concentrated in a vacuum. The conversion was determined by ^{1}H NMR analysis of the crude products.

Crystallography

X-Ray intensity data were measured at 180(2) K on a Bruker SMART APEX CCD-based diffractometer (Mo-Kα radiation, λ = 0.71073 Å) using the SMART and SAINT programs. The structures were solved by direct methods and refined on F^2 by full-matrix least-squares methods with SHELXTL version 5.1. Crystal data of Sm–**PT1**: $Sm_6(C_{27}H_{21}N_9O_3)_4(NO_3)_{18}{\cdot}5CHCl_3{\cdot}CH_3OH{\cdot}9H_2O$ ($C_{114}H_{111}Cl_{15}N_{54}O_{76}Sm_6$), M = 4887.42, hexagonal, space group $R\bar{3}$, yellow block, a = 28.803(4), c = 44.831(9) Å, V = 32211(9) Å^3, Z = 6, D_c = 1.497 g cm^{-3}, μ(Mo-Kα) = 1.890 mm^{-1}, T = 180(2) K. 11317 unique reflections [R_{int} = 0.0722]. Final R_1 [with $I > 2\sigma(I)$] = 0.0791, wR_2 (all data) = 0.2605. Non-hydrogen atoms were refined anisotropically. CCDC number: 675067. Except the solvent molecules, hydrogen atoms were fixed geometrically at calculated distances and allowed to ride on the parent non-hydrogen atoms with the isotropic displacement being fixed at 1.2 times of the atoms they attached to. Several solvent $CHCl_3$ molecules were refined with the C–Cl bond distance being fixed at 1.57 Å and Cl···Cl separation of 2.50 Å, respectively. One of the uncoordinated nitrate anions was refined with the N–O bond distance being fixed at 1.25 Å and the separation between three oxygen atoms was fixed to be the same, respectively.

Results and discussion

Structural studies of Tb–PT1 and Sm–PT1

Ligand **PT1** was synthesized according to the literature method.[14] Layering a methanol solution of $Sm(NO_3)_3{\cdot}6H_2O$ above the chloroform/methanol solution of **PT1**, like in case of the preparation of Tb–**PT1** octahedron, led to the

formation of molecular material Sm–**PT1** with the yield of 62%. Single crystal structural analysis demonstrated the formation of the octahedron Sm–**PT1**, which was similar to the reported Eu–**PT1** complex.[14] Each octahedron comprised six metal ions positioned at the vertexes, and four ligands alternatively positioned on the four of the eight faces. The separation between two metal ions bridged by one ligand was about 10.5 Å, and the distance between two diagonal metal ions was about 14.9 Å, respectively, with the inner volume being estimated as 400 $Å^3$. Each lanthanide ion was coordinated by two tridentate chelators from two different ligands and two nitrate anions, respectively. These nitrate anions were potentially removable, from which the lanthanide ions were possibly considered as coordinative unsaturated metal centers and potential acid-type catalytic active sites. These amide groups—located within the positively charged cages—provide static, geometric, coordinative, and functional properties to the cage-like capsules, which are important for the recognition of small biochemical molecules and for the base-type catalysis of special organic reactions.

Importantly, the packing patterns of the two octahedral cages in their crystals were quite different (Scheme 1). Tb–**PT1** crystallized in a space group $P\bar{3}c1$. Each octahedron positioned at a crystallographic C_3 axis and connected with three neighbors through intermolecular π···π stacking interactions, featuring a two-dimensional (6,3) sheet having a cavity of a radius of about 1.5 nm. Adjacent sheets were further packed into three-dimensional networks, exhibiting one-dimensional channels. Sm–**PT1** crystallized in a space group $R\bar{3}$. The octahedron positioned at the crystallographic C_3 axis also and connected with three neighbors through inter-molecular π···π interactions, featuring a 2D sheet similar to that of Tb–**PT1**. However, adjacent sheets in Sm–**PT1** were packed in an ABAB fashion, blocking the 1D channels. In this case, the similar molecular structure but different packing patterns of Tb–**PT1** and Sm–**PT1** made the two compounds promising candidates to optimize the heterogeneous catalysis conditions of the given reactions. TGA analysis of crystalline samples Tb–**PT1** and Sm–**PT1** showed only 18% decrease in weight for both compounds at 210 °C, corresponding to the loss of the adsorbed solvents in the crystals. These results showed that both compounds were stable enough after losing the lattice solvent molecules and could be used as catalysts in a heterogeneous manner.

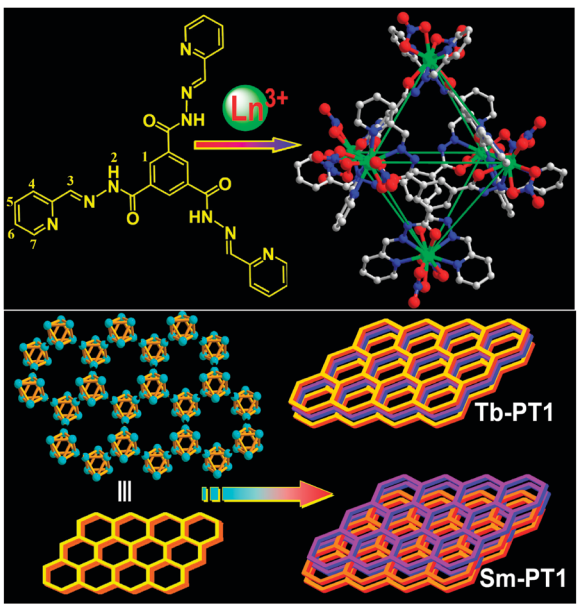

Scheme 1 Structure of ligand **PT1** and constructional fragments, showing the cationic lanthanide-based octahedral cages, and the packing diagram of the two dimensional layers consolidated by the octahedrons, showing the AAA fashion of the two-dimensional layers in the channel structure of Tb–**PT1** and the ABAB fashion of the porous-like structure of Sm–**PT1**, respectively.

Catalysis of cyanosilylation reaction of aldehydes

To understand the catalytic properties of these polyhedra and optimize the heterogeneous conditions of the given catalysts, cyanosilylation reaction provides a convenient route to cyanohydrins, which are key derivatives in the synthesis of fine chemicals and pharmaceuticals,[18] and was investigated in a heterogeneous manner. As shown in Table 1, a loading of 1 mol% of Tb–**PT1** (5 μmol) led to a 90% conversion of nitrobenzaldehydes after 1.5 h. The catalytic activity was comparable to the best prior results for MOFs.[19] Solids of Tb–**PT1** could be easily isolated from the reaction suspension by simple filtration alone and can be reused at least twice with a slight decrease in reactivity. Importantly, removal of Tb–**PT1** by filtration after only 0.5 h completely shuts down the reaction, affording only 1.8% increase in conversion upon standing for 16 h. These results demonstrated that Tb–**PT1** is a true heterogeneous catalyst. Furthermore, the conversion of 4-nitrobenzaldehyde (4-**NBA**) in a heterogeneous manner was just 11.8%, catalyzed by **PT1** (4 mol% ratio) after 1.5 h under similar experimental conditions, and the reaction didn't progress without catalyst. It seemed that the lanthanide octahedra rather than the ligand acted as the dominant catalytic active sites.

While the smooth reaction between 2-nitrobenzaldehyde (2-**NBA**) (molecular size, 5.8 × 5.3 $Å^2$), 3-nitrobenzaldehyde (3-**NBA**) (molecular size, 6.9 × 5.0 $Å^2$) or 4-**NBA** (molecular size, 7.0 × 4.3 $Å^2$) and Me_3SiCN suggested that the window size of the catalyst is larger enough to allow such kind of substrates to pass through, just 13% of the cyanosilylation product was observed when the reaction of bulky aldehyde with larger size, 3-formyl-1-phenylene-(3, 5-di-*tert*-butylbenzoate)

Table 1 Results of cyanosilylation of various aldehydes with the crystalline solids of Tb–**PT1** and Sm–**PT1**[a]

Entry	Aldehyde	Tb–**PT1** Con.[b] (%)	Sm–**PT1**Con.[b] (%)
1	4-**NBA**	90.5	79.3
2	3-**NBA**	91.6	72.3
3	2-**NBA**	95.1	77.6
4	**BA**	13.0	10.8

[a] Reaction conditions: Me_3SiCN (0.6 mmol), aldehyde (0.5 mmol), CH_2Cl_2 (0.5 mL), Tb–**PT1** or Sm–**PT1** (0.005 mmol), 20 °C, 1.5 h. [b] The conversion was determined by ^1H NMR spectroscopy.

(**BA**) (molecular size, 12.9 × 9.1 Å^2),[20] was conducted after the same period of time, in the presence of Tb–**PT1** catalyst. Given the expectation of comparable reactivity, it seems that the diameter of the channel (11.5 Å eliminating the van der Waals radii of about 3.6 Å) is too small to readily accommodate the transition state geometry required for activating the corresponding substrates. The potential size-selectivity of the cyanosilylation reactions suggested that the catalytic reactions mostly occurred in the channels of the catalysts, not on the external surface.

The investigation on the adsorption of the substrates in the catalyst also confirmed the size-selectivity. The desolvated catalyst was immersed in the solid catalyst in a CH_2Cl_2 solution containing the substrates for 3 h, and then filtrated and washed by CH_2Cl_2 several times to remove the substrate remaining on the surface. ^{1}H NMR (DMSO-d_6) of the sample immersed in the CH_2Cl_2 solution containing 4-**NBA** exhibited peaks at chemical shifts of 10.18, 8.43 and 8.17 ppm, assigned to the proton signals of the substrate, all of them being shifted downfield (δ = 0.1 ppm) (Fig. 1a–c). Detailed ^{1}H NMR spectral analyses demonstrated the 3 : 1 mole ratio of 4-**NBA** absorbed per polyhedron in the solid catalyst. However, ^{1}H NMR (DMSO-d_6) of Tb–**PT1** immersed in a CH_2Cl_2 solution containing **BA** didn't exhibit any peaks of **BA**, which asserted that the **BA** was not incorporated by the catalyst (Fig. 1d).

To further probe whether activation of the carbonyl species occurs inside the channels or on the surface of the solid catalyst, fluorescent titrations of the suspension of Tb–**PT1** in CH_2Cl_2 upon addition of the substrates were investigated. When excited at 365 nm, free Tb–**PT1** exhibited two intense emission bands of 465 nm (**PT1** emission) and 525 nm (the Tb^{3+} emission assignable to the transitions of $^5D_4 \rightarrow {}^7F_4$).[21] The addition of 4-**NBA**, 3-**NBA** and 2-**NBA** reduced the luminescence of the Tb^{3+} emission (525 nm) and **PT1** emission (465 nm) of the suspension of Tb–**PT1** in CH_2Cl_2, while both luminescence of the Tb^{3+} emission and **PT1** emission of the suspension of Tb–**PT1** were almost unaltered with the addition of **BA**. This result suggested that only the molecules having suitable sizes had the potential to enter the channels or be encapsulated by cavities, and interact with the luminescence sites from which the luminescent responses exhibited size-selective performance.

The quenching effect was rationalized by the Stern–Volmer equation:[22]

$$I_0/I = 1 + K_{SV}[M]$$

I_0 and I are the luminescence intensities of aldehyde-free Tb–**PT1** and aldehyde-incorporated Tb–**PT1**, respectively, [M] is the molar concentration of the aldehydes added, and K_{SV} is the quenching effect coefficient of the aldehyde. K_{SV} was calculated to be *ca.* 5.4 M^{-1} from the experimental data for the examined aldehyde. The addition of 4-**NBA** to Tb–**PT1** in an acetonitrile solution does not cause any obvious absorption spectroscopic changes, thus the fluorescence quenching by aldehydes should be ascribed to a PET (photo-induced energy transfer) mechanism between the guest molecules and Tb–**PT1**.[23]

Interestingly, K_{SV} values referring to the intensities at 465 nm and at 525 nm are different (Fig. 2 inset). With the decrease of the intensities of the two emission bands upon incorporating 4-**NBA**, the I_{525}/I_{465} ratio increased significantly. Since the two emission bands were isogenous, the characteristic Tb^{3+} emission was prompted by the excitation of the **PT1** group. The quenching of the two emission bands was attributed to PET from the **PT1** group to 4-**NBA**, whereas the increase of I_{525}/I_{465} ratio should be attributed reasonably to the interactions between molecules of 4-**NBA** and the Tb^{3+} ions. Accordingly, the enhancement of the emitting efficiency at 525 nm (Tb^{3+} emission) was attributed to the replacement of the coordinated solvent molecules by the aldehydes (Fig. 3). These results demonstrated that the interactions corresponding to the Tb^{3+} sites were dominant in luminescent responses ratiometrically and in activating the aldehydes.

To further validate the catalytic reactions occurring within the channels and in the surface of the catalyst, another lanthanide-based porous material Sm–**PT1** having the same

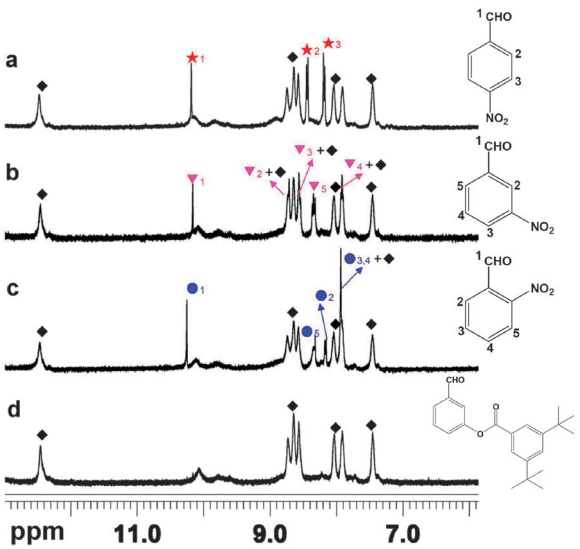

Fig. 1 ^{1}H NMR (DMSO-d_6) spectra of Tb–**PT1** that adsorbed different aldehydes: (a) 4-**NBA**, (b) 3-**NBA**, (c) 2-**NBA** and (d) **BA**. The peaks marked with a black rhombus indicate the protons in Tb–**PT1**, the others refer to the substrates.

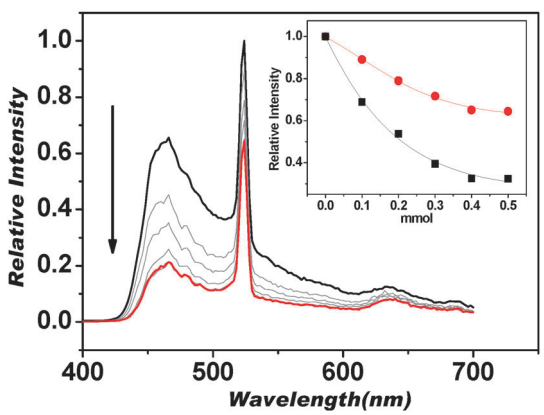

Fig. 2 Family of luminescent spectra of Tb–**PT1** emulsion in CH_2Cl_2 upon addition of various amounts of 4-**NBA** up to 0.5 mmol. The inset shows fluorescence responses of Tb–**PT1** upon addition of 4-**NBA** in CH_2Cl_2 at 525 nm (red line) and at 465 nm (black line), excitation at 365 nm.

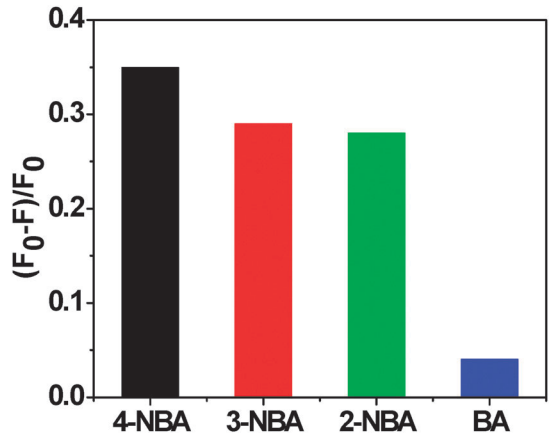

Fig. 3 Luminescent responses of Tb–**PT1** upon addition of aldehydes (0.5 mmol) of interest. Intensities were recorded at 525 nm, excitation at 365 nm.

molecular structure but a different packing pattern was investigated. Molecules of Sm–**PT1** octahedron in the crystals were packed into two-dimensional layers, but the layers stacked in an ABAB fashion to block the channels into cavities. The sorption experiments including the ^{1}H NMR (d_6-DMSO) of the immersed sample suggested the same absorption of substrate 4-**NBA** within Sm–**PT1**, and revealed the presence of 3 mole equiv. of 4-**NBA** per polyhedron. The loading of only 1 mol% ratio of Sm–**PT1** (5 μmol) led to excellent conversion of the nitrobenzaldehyde substrates, whereas the conversions of the corresponding reactions catalyzed by Sm–**PT1** were lower compared to the reactions prompted by Tb–**PT1**. And the conversion of cyanosilylation with **BA** catalyzed by Sm–**PT1** was the lowest one and almost the same as that by Tb–**PT1**, while the conversion of all the entries was over 97% using $Tb(NO_3)_3$ and $Sm(NO_3)_3$ as catalysts under the same reaction conditions, respectively. Because the two compounds have similar molecular structures and almost the same coordination geometry, the difference in the reaction conversions might be one of the indicators that the reactions occurred within the channels or pores of the catalysts. The higher conversion of the channel structure Tb–**PT1** compared to that of the porous structure Sm–**PT1** suggested that the presence of nanometre channels might benefit the nitrobenzaldehydes diffusing swiftly through the channels and accommodating the transition state geometry required for activating these substrates.

Catalyses of aldol reaction by Tb–PT1 and Sm–PT1

As mentioned in the literature, the amide groups seemed basic enough to abstract an α-H atom of a ketone to generate a nucleophilic enolate.[24] Aldol reaction, one of the most powerful carbon–carbon bond-forming reactions,[25] was chosen to optimize the heterogeneous catalytic conditions of these octahedra.[26] As shown in Table 2, the loading of only 2 mol% ratio of Tb–**PT1** (0.01 mmol) led to 80% conversion corresponding to 4-**NBA** and cyclohexanone with the diastereo-selectivity being 2 : 1 (*syn* : *anti*). And the catalysis efficiency of Tb–**PT1** was comparable to the best prior result for metal–organic framework catalysts.[27]

Furthermore, in the heterogeneous manner the conversion of 4-**NBA** and cyclohexanone was just 4.8% with only *cis*

Table 2 Aldol reactions of cyclohexanone and various aldehydes with Sm–**PT1** and Tb–**PT1**[a]

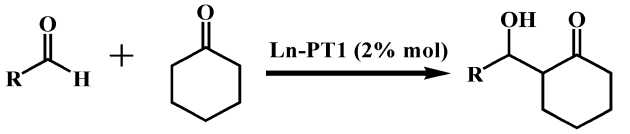

		Tb–**PT1**		Sm–**PT1**		**PT1**	
Entry	Substrate	Con.%	Dr(s/a)	Con.%	Dr(s/a)	Con.%	Dr(s/a)
5	4-**NBA**	80.5	2.0 : 1	64.9	2.1 : 1	4.8	*syn*
6	3-**NBA**	75.2	1.7 : 1	56.0	2.3 : 1	8.9	*syn*
7	2-**NBA**	48.2	2.1 : 1	31.5	1.4 : 1	8.3	*syn*
8	**BA**	27.5	2.4 : 1	21.3	2.4 : 1	9.1	*syn*

[a] The reaction was carried out at 37 °C for 5 d with cyclohexanone (5 mmol), aldehyde (0.5 mmol) and 0.01 mmol catalysts (2 mol%) in CH_3OH/H_2O, the conversion and diastereomer were determined by ^{1}H NMR spectroscopy.

isomer catalyzed by **PT1** (8 mol% ratio) under the same conditions. Tb–**PT1** solids could also be easily isolated from the reaction suspension by simple filtration alone and can be reused at least twice with a slight decrease in reactivity. Whereas the conversions of other two nitrobenzaldehydes with different dimensions (75.2% and 48.2%) were much lower than 4-**NBA** prompted by Tb–**PT1**, only 27.5% of the aldol product was observed in the case of the bulky aldehyde **BA** as substrate after the same period of time in the presence of Tb–**PT1**. While the sorption investigation and the catalytic cyanosilylation reactions of various aldehydes with the crystalline solids of Tb–**PT1** suggested that molecules of all the three nitrobenzaldehydes could smoothly pass through the channels of the catalysts. The lower catalytic effect in the case of 2-, or 3- nitrobenzaldehydes as substrates should be likely attributed to that the size of the opening regular trigon within the octahedral molecule is too small for them to enter the inner cavities of the octahedra themselves, even considering the possible difference in their reactive activity. Accordingly, we think that the aldol reactions should take place within the octahedral cavities, and distinguish conversions rooted in the size of the opening regular trigon having an edge of about 10 Å^2 within the octahedral molecule.

To further validate the potential catalytic mechanism and probe whether activation of the carbonyl species occurs inside the inner cavities of the polyhedron or in the channels/on the surface of the solid catalyst, fluorescent titration of the suspension of Tb–**PT1** in CH_2Cl_2 upon addition of the cyclohexanone was investigated. As mentioned above, the Uv-vis spectra of Tb–**PT1** do not have any significant absorption variation upon addition of 4-**NBA** even at high concentration. However, the addition of cyclohexanone led to the significant absorbance decrease at the peaks 330 nm and 365 nm, and caused the appearance of a new peak at about 415 nm (Fig. 4). The presence of sharp isosbestic points at about 400 nm and 350 nm indicates that only two species coexist in the equilibrium. Since the bands at 330 nm and 415 nm were mainly attributed to the ligand-based charge transfer bands,[14] the absorption variations of the catalyst were mainly attributed to the potential interactions corresponding to the amide group. Importantly, the addition of cyclohexanone to the suspension of Tb–**PT1** in

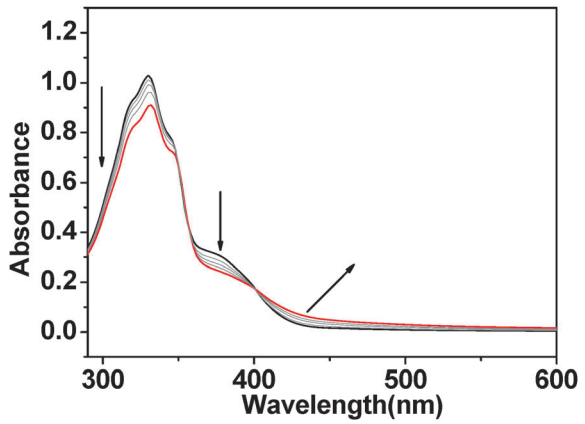

Fig. 4 Uv-vis spectra of the Tb–**PT1** (5×10^{-6} M) upon addition of cyclohexanone (0.25 mM) to an acetontrile solution (a); Luminescent responses of Tb–**PT1** upon addition of cyclohexanone (0.1 mL to 0.5 mL).

CH_2Cl_2 caused luminescence enhancement of the Tb^{3+} emission (525 nm) and ligand-based emission (465 nm) significantly (Fig. 5). As the two bands were isogenous, and the characteristic Tb^{3+} emission was prompted by the excitation of the **PT1** group, the luminescent enhancements of the two emission bands were reasonably attributed to interactions between the cyclohexanone and the amide groups in the ligand backbone. Clearly, these results revealed that the interactions between cyclohexanone and the solid of the catalyst were mainly taking place at the active sites on the ligand backbone, mainly attributed to the potential hydrogen bonding between the cyclohexanone molecules and amide groups.

Interestingly, under the same experimental conditions, the loading of only 2 mol% ratio of Sm–**PT1** (0.01 mmol) catalyst led to 65% conversion corresponding to 4-**NBA** with the diastereoselectivity of 2 : 1 (*syn* : *anti*). The 21.3%/27.5% conversion (entry 8) in the presence of Sm–**PT1**/Tb–**PT1** suggested that the narrow triangle opening of these molecular polyhedra was too small for **BA** to pass through. The almost same conversion and the same size-selective sequence of the two catalysts confirmed that the aldol reactions should take place within the octahedral cavities,

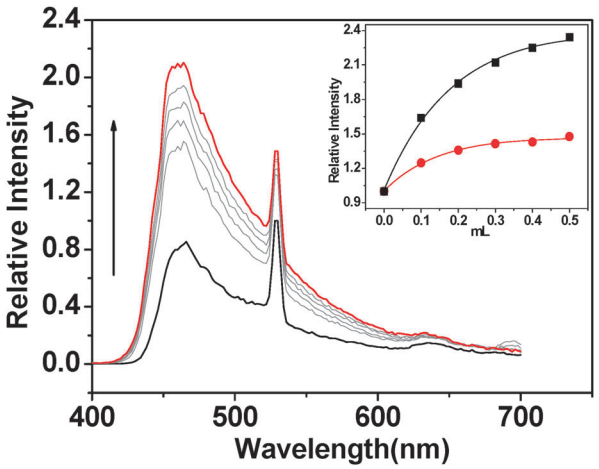

Fig. 5 Fluorescence responses of Tb–**PT1** upon addition of cyclohexanone in CH_2Cl_2 at 525 nm (red line) and at 465 nm (black line). Excitation at 365 nm (inset).

given that the two compounds have similar molecular structures and almost the same coordination geometry, but different packing patterns. While the immobilization of unsaturated Lewis acid Ln ions within the relatively open frameworks having well-defined pores represents extensively investigated methodologies and enables researchers to target some unique porous LnMOFs with multi-functional properties and catalytic applications.[28] The heterogeneous catalytic behavior of our materials is quite significant, it not only suggests that the porous molecular materials comprised of semi-infinite macrocycles have the potential to combine the excellent size discrimination properties of the macrocycles in solution and the advantage of the heterogeneous catalysts, but also demonstrates that the catalysts containing unsaturated lanthanide ions positioned at the intermolecular cavities of the crystals and amide groups within the inner cavities of the polyhedron have the potential to exhibit both base-type and acid-type catalytic driving forces directly. And owing to the different catalytic mechanisms, our systems also provide the possibility to tune the size-selectivity through controlling the catalytic reactions within the inner cavities of the discrete molecular polyhedron or within the intermolecular channels or pores of the materials consolidated.

The as-synthesized crystals of polyhedra lost part of their lattice molecules under ambient conditions. However, when the desolvated amorphous powders were reacted, they were restored to the original crystalline phase, which was detected by the XRPD patterns. Crystalline solids of the two compounds were also easily isolated from the reaction suspension by filtration alone and can be reused at least twice without loss of activity. The maintenance of the crystalline information of the solid compounds during the reaction processes suggested the possibility of the powder to be recycled with a comparable catalytic activity.

Conclusions

In summary, we reported the catalytic properties of multi-functional lanthanide–organic octahedra Tb–**PT1** and Sm–**PT1** featuring both Lewis acidic Ln^{3+} sites and basic amide group sites. These molecular materials catalyze the cyanosilylation and aldol reactions in a size-selective fashion through base-type and acid-type catalysis sites, respectively. Crystalline solids of the catalysts were easily isolated from the reaction suspension by filtration alone and can be reused without loss of activity, suggesting that the catalysts were recycled. The size-selective behaviors coupled with the guest–host spectroscopic investigation between the reaction substrates and the catalyst suggested that the cyanosilylation reactions mostly took part in the channel of the catalysts and the aldehydes substrates were activated by the Ln^{3+} ions, while the aldol reactions mainly occurred in the octahedral cavities and the cyclohexanone substrates possibly interacted with the amide groups through a hydrogen bond, respectively. These crystalline molecular materials hierarchically assembled from semi-infinite metal–organic polyhedra are thus expected to be useful catalysts which could combine the advantage of a heterogeneous catalyst and the excellent size discrimination properties of the polyhedra in solution. The efficient approach will be extended to other lanthanide-based polyhedra systems having both coordination unsaturated metal centers and a

series of organic active sites to hierarchically assemble more efficient acid- and/or base-type porous heterogeneous catalysts of organic synthetic interest.

Acknowledgements

This work is supported by the National Natural Science Foundation of China (20801008).

Notes and references

1 (*a*) B. Olenyuk, J. A. Whiteford and P. J. Stang, *Nature*, 1999, **398**, 796–799; (*b*) N. Takeda, K. Umemoto, K. Yamaguchi and M. Fujita, *Nature*, 1999, **398**, 794–796; (*c*) D. J. Tranchemontagne, Z. Ni, M. O'Keeffe and O. M. Yaghi, *Angew. Chem., Int. Ed.*, 2008, **47**, 5136–5147; (*d*) J.-R. Li and H.-C. Zhou, *Nat. Chem.*, 2010, **2**, 893.

2 (*a*) F. Hof and J. Rebek, Jr., *Proc. Natl. Acad. Sci. U. S. A.*, 2002, **99**, 4775–4777; (*b*) M. D. Pluth, R. G. Bergman and K. N. Raymond, *Science*, 2007, **316**, 85–88; (*c*) M. Jung, H. Kim, K. Baek and K. Kim, *Angew. Chem., Int. Ed.*, 2008, **47**, 5755–5757; (*d*) T. K. Ronson, J. Fisher, L. P. Harding, P. J. Rizkallah, J. E. Warren and M. J. Hardie, *Nat. Chem.*, 2009, **1**, 212–216.

3 (*a*) D. L. Caulder and K. N. Raymond, *Acc. Chem. Res.*, 1999, **32**, 975–982; (*b*) S. Leininger, B. Olenyuk and P. J. Stang, *Chem. Rev.*, 2000, **100**, 853–908; (*c*) M. Fujita, K. Umemoto, M. Yoshizawa, N. Fujita, T. Kusukawa and K. Biradha, *Chem. Commun.*, 2001, 509–518; (*d*) R. M. McKinlay, G. W. V. Cave and J. L. Atwood, *Proc. Natl. Acad. Sci. U. S. A.*, 2005, **102**, 5944–5948.

4 (*a*) N. C. Gianneschi, M. S. Maser and C. A. Mirkin, *Acc. Chem. Res.*, 2005, **38**, 825–837; (*b*) T. D. Hamilton, G. S. Papaefstathiou, T. Friscic, D. K. Bucar and L. R. MacGillivray, *J. Am. Chem. Soc.*, 2008, **130**, 14366–14367.

5 (*a*) P. J. Stang and B. Olenyuk, *Acc. Chem. Res.*, 1997, **30**, 502–518; (*b*) S. R. Seidel and P. J. Stang, *Acc. Chem. Res.*, 2002, **35**, 972–983; (*c*) S. J. Dalgarno, N. P. Power and J. L. Atwood, *Coord. Chem. Rev.*, 2008, **252**, 825–841; (*d*) M. Yoshizawa, J. K. Klosterman and M. Fujita, *Angew. Chem., Int. Ed.*, 2009, **48**, 3418–3438.

6 (*a*) D. L. Caulder and R. N. Raymond, *Acc. Chem. Res.*, 1999, **32**, 975–982; (*b*) D. Fiedler, D. H. Leung, R. G. Bergman and K. N. Raymond, *Acc. Chem. Res.*, 2005, **38**, 349–358; (*c*) R. W. Saalfrank, H. Maid and A. Scheurer, *Angew. Chem., Int. Ed.*, 2008, **47**, 8794–8824; (*d*) P. Mal, B. Breiner, K. Rissanen and J. R. Nitschke, *Science*, 2009, **324**, 1697–1699.

7 M. D. Pluth, R. G. Bergman and K. N. Raymond, *Science*, 2007, **316**, 85–88.

8 M. Yoshizawa, M. Tamura and M. Fujita, *Science*, 2006, **312**, 251–254.

9 (*a*) J. Meeuwissen and J. N. H. Reek, *Nat. Chem.*, 2010, **2**, 615–621; (*b*) T. S. Koblenz, J. Wassenaar and J. N. H. Reek, *Chem. Soc. Rev.*, 2008, **37**, 247–262; (*c*) P. W. N. M. Van Leeuwen, *Supramolecular Catalysis*, Wiley-VCH, 2008.

10 (*a*) M. Heitbaum, F. Glorius and I. Escher, *Angew. Chem., Int. Ed.*, 2006, **45**, 4732; (*b*) *Principles and Practice of Heterogeneous Catalysis*, ed. J. M. Thomas and W. J. Thomas, Wiley-VCH, Weinheim, 1997; (*c*) H.-U. Blaser, B. Pugin and M. Studer, in *Chiral Catalyst Immobilization and Recycling*, ed. D. E. DeVos, I. F. J. Vankelecom and P. A. Jacobs, Wiley-VCH, Weinheim, 2000, p. 1.

11 (*a*) J. Y. Lee, O. K. Farha, J. K. Roberts, A. Scheidt, S. B. T. Nguyen and J. T. Hupp, *Chem. Soc. Rev.*, 2009, **38**, 1450–1459; (*b*) L. Q. Ma, C. Abney and W. B. Lin, *Chem. Soc. Rev.*, 2009, **38**, 1248–1256.

12 (*a*) J. I. García, B. López-Sánchez and J. A. Mayoral, *Org. Lett.*, 2008, **10**, 4995–4998; (*b*) S. H. Cho, B. Q. Ma, S. T. Nguyen, J. T. Hupp and T. E. Albrecht-Schmitt, *Chem. Commun.*, 2006, 2563–2564.

13 (*a*) V. Chandrasekhar, P. Thilagar, J. F. Bickley and A. Steiner, *J. Am. Chem. Soc.*, 2005, **127**, 11556–11557; (*b*) G. Li, W.-B. Yu and Y. Cui, *J. Am. Chem. Soc.*, 2008, **130**, 4582–4583; (*c*) Y. Liu, R. Zhang, C. He, D. B. Dang and C. Y. Duan, *Chem. Commun.*, 2010, **46**, 746–748.

14 C. He, Z. H. Lin, Z. He, C. Y. Duan, C. H. Xu, Z. M. Wang and C. H. Yan, *Angew. Chem., Int. Ed.*, 2008, **47**, 877–881.

15 D. Moon, S. Kang, J. Park, K. Lee, R. P. John, H. Won, G. H. Seong, Y. S. Kim, G. H. Kim, H. Rhee and M. S. Lah, *J. Am. Chem. Soc.*, 2006, **128**, 3530–3531.

16 (*a*) S. Hasegawa, S. Horike, R. Matsuda, S. Furukawa, K. Mochizuki, Y. Kinoshita and S. Kitagawa, *J. Am. Chem. Soc.*, 2007, **129**, 2607–2614; (*b*) Y. Zou, M. Park, S. Hong and M. S. Lah, *Chem. Commun.*, 2008, 2340–2342.

17 (*a*) X. Xu, M. Ma, Y. Yao, Y. Zhang and Q. Shen, *Eur. J. Inorg. Chem.*, 2005, 676–684; (*b*) T. N. Parac-Vogt, S. Pachini, P. Nockemann, K. V. Hecke, L. V. Meervelt and K. Binnemans, *Eur. J. Org. Chem.*, 2004, 4560–4566.

18 (*a*) K. Higuchi, M. Onaka and Y. Izumi, *Bull. Chem. Soc. Jpn.*, 1993, **66**, 2016–2032; (*b*) R. J. H. Gregory, *Chem. Rev.*, 1999, **99**, 3649–3682; (*c*) M. North, *Tetrahedron: Asymmetry*, 2003, **14**, 147–176.

19 (*a*) M. Fujita, Y. J. Kwon, S. Washizu and K. Ogura, *J. Am. Chem. Soc.*, 1994, **116**, 1151–1152; (*b*) O. R. Evans, H. L. Ngo and W. B. Lin, *J. Am. Chem. Soc.*, 2001, **123**, 10395–10396; (*c*) K. Schlichte, T. Kratzke and S. Kaskel, *Microporous Mesoporous Mater.*, 2004, **73**, 81–88; (*d*) S. Horike, M. Dinca, K. Tamaki and J. R. Long, *J. Am. Chem. Soc.*, 2008, **130**, 5854–5855; (*e*) S. Neogi, M. K. Sharma and P. K. Bharadwaj, *J. Mol. Catal. A: Chem.*, 2009, **299**, 1–4.

20 These molecular sizes are calculated based on the Chem Office soft.

21 (*a*) Z. Li, G. Zhu, X. Guo, X. Zhao, Z. Jin and S. Qiu, *Inorg. Chem.*, 2007, **46**, 5174–5178; (*b*) B. Zhao, X. Y. Chen, P. Cheng, D. Z. Liao, S. P. Yan and Z. H. Jiang, *J. Am. Chem. Soc.*, 2004, **126**, 15394–15395; (*c*) B. Chen, L. Wang, F. Zapata, G. Qian and E. B. Lobkovsky, *J. Am. Chem. Soc.*, 2008, **130**, 6718–6719; (*d*) K.-L. Wong, G.-L. Law, Y.-Y. Yang and W.-T. Wong, *Adv. Mater.*, 2006, **18**, 1051–1054.

22 (*a*) Y. Xiao, Y. Cui, Q. Zheng, S. Xiang, G. Qian and B. Chen, *Chem. Commun.*, 2010, **46**, 5503–5505; (*b*) B. Chen, L. Wang, Y. Xiao, F. R. Fronczek, M. Xue, Y. Cui and G. Qian, *Angew. Chem., Int. Ed.*, 2009, **48**, 500–503.

23 (*a*) P. Jiang and Z. Guo, *Coord. Chem. Rev.*, 2004, **248**, 205–229; (*b*) R. Kramer, *Angew. Chem., Int. Ed.*, 1998, **37**, 772–773; (*c*) L. Fabbrizzi, M. Licchelli, P. Pallavicini, A. Perotti, A. Taglietti and D. Sacchi, *Chem.–Eur. J.*, 1996, **2**, 75–82; (*d*) M. Boiocchi, L. Fabbrizzi, M. Licchelli, D. Sacchi, M. Vazquez and C. Zampa, *Chem. Commun.*, 2003, 1812–1813.

24 (*a*) C. M. Lee and W. D. Kumler, *J. Am. Chem. Soc.*, 1962, **84**, 571–578; (*b*) H. A. Bent, *Chem. Rev.*, 1968, **68**, 587–648; (*c*) P. L. Huyskens, *J. Am. Chem. Soc.*, 1977, **99**, 2578–2582.

25 (*a*) L. G. Wade, *Organic Chemistry*, Prentice Hall, Upper Saddle River, New Jersey, 6th edn, 2005, pp. 1056–1066; (*b*) M. B. Smith and J. March, *Advanced Organic Chemistry*, Wiley Interscience, New York, 5th edn, 2001, pp. 1218–1223; (*c*) R. Mahrwald, *Modern Aldol Reactions*, Wiley-VCH Verlag GmbH & Co. KGaA., Weinheim, Germany, 2004, vol. 1 and 2, pp. 1218–1223.

26 (*a*) A. Olmos, A. Alix, J. Sommer and P. Pale, *Chem.–Eur. J.*, 2009, **15**, 11229–11234; (*b*) S. Luo, J. Li, L. Zhang, H. Xu and J. P. Cheng, *Chem.–Eur. J.*, 2008, **14**, 1273–1281.

27 (*a*) M. Banerjee, S. Das, M. Yoon, H. J. Choi, M. H. Hyun, S. M. Park, G. Seo and K. Kim, *J. Am. Chem. Soc.*, 2009, **131**, 7524–7525; (*b*) S. K. Ghosh, S. Bureekaew and S. Kitagawa, *Angew. Chem., Int. Ed.*, 2008, **47**, 3403–3406.

28 (*a*) M. Gustafsson, A. Bartoszewicz, B. Martin-Matute, J. L. Sun, J. Grins, T. Zhao, Z. Y. Li, G. S. Zhu and X. D. Zou, *Chem. Mater.*, 2010, **22**, 3316–3322; (*b*) S. Kitagawa, S. I. Noro and T. Nakamura, *Chem. Commun.*, 2006, 701–707; (*c*) O. R. Evans, H. L. Ngo and W. Lin, *J. Am. Chem. Soc.*, 2001, **123**, 10395–10396; (*d*) N. Snejko, C. Cascales, B. Gomez-Lor, E. Gutiérrez-Puebla, M. Iglesias, C. Ruiz-Valero and M. A. Monge, *Chem. Commun.*, 2002, 1366–1367; (*e*) J. W. Han and C. L. Hill, *J. Am. Chem. Soc.*, 2007, **129**, 15094–15095; (*f*) T. Dewa, T. Saiki and Y. Aoyama, *J. Am. Chem. Soc.*, 2001, **123**, 502–503.